Taylor & Francis
Taylor & Francis Group

Science and Technology of Advanced Materials: Methods

ISSN: 2766-0400 (Online) Journal homepage: www.tandfonline.com/journals/tstm20

Fabrication of β-Ga_2O_3/air-gap structures on (001) β-Ga_2O_3 using HCl gas etching

Takayoshi Oshima & Yuichi Oshima

To cite this article: Takayoshi Oshima & Yuichi Oshima (2025) Fabrication of β-Ga_2O_3/air-gap structures on (001) β-Ga_2O_3 using HCl gas etching, Science and Technology of Advanced Materials: Methods, 5:1, 2554046, DOI: 10.1080/27660400.2025.2554046

To link to this article: https://doi.org/10.1080/27660400.2025.2554046

Published online: 03 Sep 2025.

SCIENCE AND TECHNOLOGY OF ADVANCED MATERIALS: METHODS
2025, VOL. 5, NO. 1, 2554046
https://doi.org/10.1080/27660400.2025.2554046

Fabrication of β-Ga_2O_3/air-gap structures on (001) β-Ga_2O_3 using HCl gas etching

Takayoshi Oshima and Yuichi Oshima

Research Center for Electronic and Optical Materials, National Institute for Materials Science, Tsukuba, Japan

ABSTRACT

β-Ga_2O_3/air-gap structures were fabricated on (001) substrates via crystallographic etching with HCl gas. Etching at 650 °C under an HCl partial pressure of 250 Pa resulted in a vertical etch rate of 0.10 μm/min on the (001) plane and a lateral etch rate of 0.70 μm/min along the < 010 > direction. This high orthogonal etching anisotropy enabled the formation of β-Ga_2O_3/air-gap structures – such as cantilevers and air bridges – without the need for wafer bonding or transfer processes. This straightforward technique, compatible with commonly used (001) substrates, holds promise for the integration of β-Ga_2O_3-based microelectromechanical systems (MEMS) and power electronic devices.

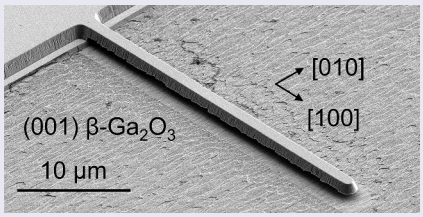

IMPACT STATEMENT

β-Ga_2O_3/air-gap structures were directly fabricated on (001) orientation β-Ga_2O_3 substrates using crystallographic HCl gas etching, offering strong potential for monolithic integration of β-Ga_2O_3-based microelectromechanical systems (MEMS) and power electronic devices.

ARTICLE HISTORY
Received 30 May 2025
Revised 18 July 2025
Accepted 24 August 2025

KEYWORDS
β-Ga_2O_3; cantilever; air bridge; MEMS; crystallographic etching; HCl gas etching

1. Introduction

β-Ga_2O_3 is an emerging wide bandgap semiconductor with great potential for a wide range of applications. It offers both a high critical breakdown field of nearly 8 MV cm^{-1} and compatibility with melt growth techniques for producing high-quality, scalable wafers [1,2]. Owing to these two major advantages over conventional wide bandgap semiconductors – such as SiC, GaN, and diamond—β-Ga_2O_3 is increasingly regarded as a promising material for next-generation low-loss, high-voltage power devices [3]. In addition, β-Ga_2O_3 demonstrates native solar-blind photoresponsivity and gas sensitivity, which are beneficial for developing filterless solar-blind photodetectors and gas sensors, respectively [4,5]. It also possesses favorable mechanical properties, including a high Young's modulus (~261 GPa) and a high acoustic velocity (~6623 m s^{-1}), both comparable to those of Si, rendering it well-suited for microelectromechanical systems (MEMS) applications [6]. These properties suggest that β-Ga_2O_3 could serve as a highly versatile platform for future electromechanically coupled and tunable devices in electronics, optoelectronics, and advanced sensing. Potential applications include radio-frequency MEMS components in high-power, high-frequency systems for defense, wireless infrastructure, satellites, and resonance-enhanced solar-blind UV photodetectors and gas sensors [6].

For the monolithic integration of β-Ga_2O_3-based MEMS components into the aforementioned β-Ga_2O_3-based systems, it is preferable to fabricate mechanically suspended β-Ga_2O_3/air-gap structures – such as cantilevers and air bridges – directly on β-Ga_2O_3 substrates. However, previously reported MEMS devices from other groups have employed β-Ga_2O_3 /air-gap structures formed by manually exfoliating narrow flakes and membranes from bulk single crystals, followed by their transfer onto foreign substrates [7–12]. Even when transferred onto pre-patterned β-Ga_2O_3 substrates, such a low-reproducibility, human-

CONTACT Takayoshi Oshima OSHIMA.Takayoshi@nims.go.jp Research Center for Electronic and Optical Materials, National Institute for Materials Science (NIMS), 1-1 Namiki, Tsukuba, Ibaraki 305-0044, Japan

dependent method is unsuitable for practical applications. The advanced ion-cutting technique could potentially offer a solution to this reproducibility issue [13]. Nevertheless, the process is inherently complex, involving hydrogen ion implantation, wafer bonding, low-temperature annealing to induce blistering, and layer splitting, followed by chemical mechanical polishing and high-temperature annealing to recover crystallinity. Therefore, an alternative reproducible method that avoids such complexity while enabling direct air-gap formation on β-Ga_2O_3 substrates is highly desirable.

As a simpler and more direct approach, we propose a crystallographic gas etching technique. Since 2023, we have demonstrated anisotropic etching of single-crystal β-Ga_2O_3 substrates with various orientations – including (001), (010), ($\bar{1}$02), (011), and (100) – using N_2-diluted HCl gas and forming gas, without the need for plasma excitation [14–20]. Unlike conventional plasma-based dry etching, these etching methods do not cause plasma-induced damage to the crystal. The resulting etched structures were bounded by crystal facets with lower surface energy densities. Among these, the (100) plane, known to possess the lowest surface energy density [21], exhibited the highest etch resistance and consistently emerged across all substrate orientations. Leveraging this strong anisotropic etching behavior, we recently succeeded in forming air-gap structures to form air bridges on (100) substrates [20]. This achievement was enabled by a highly orthogonal etching rate ratio: the lateral etch rate along the [010] was approximately ten times greater than the vertical etch rate on the (100) plane.

However, the (100) plane is unsuitable for homoepitaxial growth due to the formation of twin lamellae due to the double positioning of adatoms – a phenomenon where adatoms may occupy symmetrically equivalent sites leading to twin boundaries [22]. Although this issue can be mitigated by using miscut substrates or applying surfactant-assisted growth within a narrow growth window [22–24], research on (100) substrates still significantly lags behind that on (001) and (010) substrates. The latter orientations naturally support single-domain homoepitaxy without the need for additional techniques. In particular, for the (001) orientation, 4-inch single-crystal wafers with lightly doped, thick homoepitaxial layers are commercially available, facilitating the fabrication of vertical power devices with superior performance [3,25]. Thus, the formation of β-Ga_2O_3/air-gap structures on (001) substrates is highly desirable to ensure compatibility with the most advanced device platform.

In a previous study, we investigated the HCl gas etching characteristics on the (001) plane using etching masks with various etching geometries, and systematically varied key process parameters, including the HCl partial pressure (P_{HCl} = 25–250 Pa) and process temperature (T_P = 548–949 °C) [15]. We observed that the lateral-to-vertical etch rate ratio increased with increasing P_{HCl} and decreasing T_P, with lateral etching being most pronounced along the < 010 > direction at lower T_P. These findings suggest that air-gap formation with crystallographic etching is possible even for (001) substrates.

In this study, therefore, we conducted HCl gas etching on (001) β-Ga_2O_3 substrates under conditions of high P_{HCl} of 250 Pa and low T_P of 650 °C. The resulting lateral-to-vertical etch rate ratio reached as high as 7, enabling the fabrication of cantilevers and air-bridge structures, which are commonly employed in MEMS applications.

2. Experimental

We conducted etching experiments based on the processes and measurement methods described below. The SiO_2 mask layer was deposited on the β-Ga_2O_3 surface using plasma-enhanced chemical vapor deposition (PECVD) with tetraethoxysilane (TEOS) and O_2 as precursors. Conventional capacitively coupled plasma reactive ion etching (CCP-RIE) with fluorine chemistry (CHF_3 and N_2) and inductively coupled plasma reactive ion etching (ICP-RIE) with chlorine chemistry (BCl_3 and Ar) were used to etch the SiO_2 mask and β-Ga_2O_3 substrate, forming etching windows and mesa structures, respectively. Laser lithography with a 375-nm semiconductor laser was employed to define the CCP-RIE and ICP-RIE regions. The photoresist mask was removed by cleaning with organic solvents (N-methyl-2-pyrrolidone and isopropyl alcohol) and oxygen plasma treatment in a parallel-plate plasma system. HCl gas etching was carried out in a custom-built halide vapor phase epitaxy/etching system. The etching process was performed in an N_2-diluted HCl gas flow under atmospheric pressure, with relatively high P_{HCl} of 250 Pa and low T_P of 650 °C. The gas flow was directed perpendicular to the substrate, which was mounted on a rotating holder. The SiO_2 thickness was measured by ellipsometry. The SiO_2 mask was removed using buffered hydrofluoric acid (BHF). The etched structures were observed using differential interference contrast (DIC) microscopy and scanning electron microscopy (SEM). A focused ion beam (FIB)-SEM hybrid system was also employed for cross-sectional imaging, with a carbon layer deposited prior to FIB milling to preserve the surface structure. A low acceleration voltage of 2.0 kV was used for all SEM observations to enhance material contrast. Etch depths were measured with a stylus profilometer or the FIB-SEM system.

3. Results and discussion

3.1. Crystallographic etching on (001)

First, HCl gas etching was performed on a planar (001) β-Ga_2O_3 substrate. The process sequence is illustrated in Figure 1. A 151-nm-thick SiO_2 layer was deposited by PECVD and patterned using laser lithography and CCP-RIE to form etching windows. The window shapes included a rectangle and two types of wagon-wheel patterns. The size of the rectangular window was 100 μm × 200 μm. The wagon-wheel patterns consisted of line-shaped windows, each measuring 50 μm in length and 0.64 μm in width. One configuration included 36 windows arranged at 10° intervals. The other configuration featured windows aligned along specific crystallographic directions, which are parallel to the nearly vertical low Miller-index oxygen sublattice planes of (100), (010), (310), and ($\bar{3}$10). HCl gas etching of the masked substrate was then carried out for 10 min.

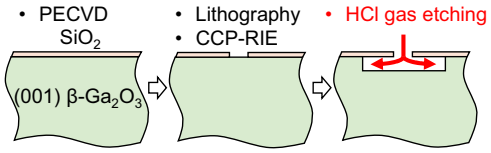

Figure 1. Process sequence for selective-area HCl gas etching on the (001) β-Ga_2O_3 substrate.

The etched structures were examined to investigate the in-plane anisotropic etching nature. By measuring the etched depth within the rectangular window, the vertical etch rate was determined to be 0.10 μm min^{-1}. In contrast, the side etching exhibited a strong dependence on in-plane orientation, as observed in the DIC images of the two wagon-wheel patterns Figure 2(a) and 2(b), where the side-etched regions are visualized by distinctive colors, in contrast to the gray-toned masked areas. The magnified DIC image of the line-shaped window aligned along the [100] direction clearly shows the color distinctions among the mask, window, and side-etched regions Figure 2(c). Side etching was most enhanced when the windows were

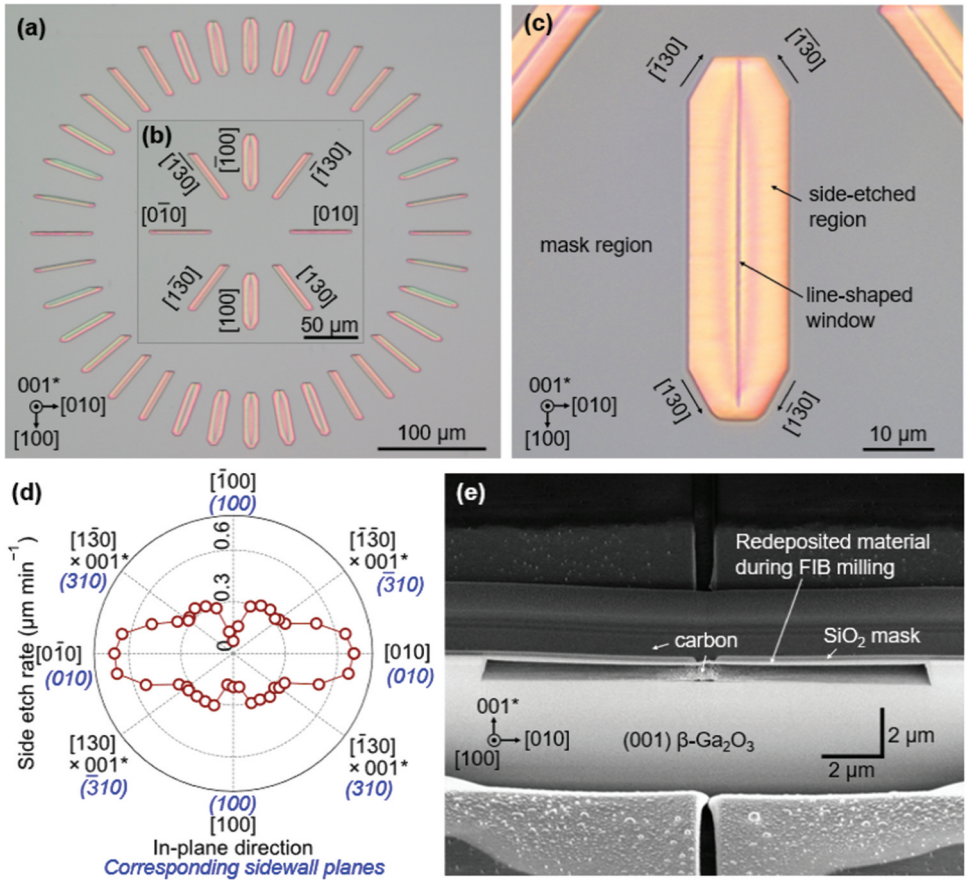

Figure 2. Summary of the in-plane dependence of side etching characteristics on the (001) β-Ga_2O_3 substrate. (a)–(c) DIC microscope images of side-etched structures formed beneath the wagon-wheel window patterns. The line-shaped windows were arranged at 10° intervals from the [010] direction in (a), whereas in (b) they were aligned along specific crystallographic directions parallel to the low-index oxygen sublattice planes. (a) and (b) were recorded at the same magnification. (c) Magnified image of the region near the line-shaped window aligned with the [100] direction. (d) Polar plot of side etch rates perpendicular to the wagon-wheel windows shown in (a) and (b). '*' and '×' denotes the reciprocal lattice vector and cross product, respectively. (e) 54° tilted-view SEM image of the cross section of the etched structure formed beneath the line-shaped window in the [100] direction, which corresponds to the structure shown in (c).

aligned with the [100] direction and least pronounced along the [010] direction. It was also suppressed for windows oriented along [130] and [1 $\bar{3}$0]. These window directions are parallel to the aforementioned oxygen sublattice planes, suggesting that the oxygen sublattice strongly influences the gas etching process. The side etch rates measured from the wagon-wheel patterns were plotted in polar coordinates, as shown in Figure 2(d). The resulting pattern closely reflects the symmetry of the β-Ga_2O_3 crystal structure [26], which exhibits mirror symmetry with respect to the (010) plane and two-fold rotational symmetry around the [010] axis. These symmetries explain why right and left halves of the plot display mirror symmetry, while upper and lower halves exhibit quasi-mirror symmetry. The maximum side etch rate of 0.70 μm min^{-1} in the [010] and [0 $\bar{1}$0] directions – which are crystallographically equivalent – is seven times higher than the vertical etch rate of 0.10 μm min^{-1} on the (001) plane. The cross-sectional profile of the etched trench in the [100]-oriented window, corresponding to that shown in Figure 2(c), was observed using the FIB-SEM system Figure 2(e). The etched trench primarily extended in the [010] and [0 $\bar{1}$0] lateral directions, while its depth remained relatively shallow. The high lateral-to-vertical etching selectivity is considered to enable the formation of air gaps using the etching process alone, eliminating the need for wafer bonding and transfer processes.

3.2. Fabrication of β-Ga_2O_3/air-gap structures

Next, cantilevers and air bridges – fundamental MEMS components – were fabricated on a (001) β-Ga_2O_3 substrate. The process flow is schematically illustrated in Figure 3. First, mesa etching was performed to define the cantilever and air bridge areas via laser lithography and ICP-RIE. The mesas were oriented along the [100] direction so that their sidewalls faced the [010] and [0 $\bar{1}$0] directions. Their dimensions were 0.92 μm in height, ~1.7 μm in width, and ~30.0 μm in length.

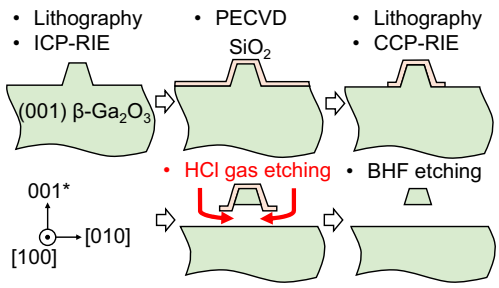

Figure 3. Process sequence for the fabrication of β-Ga_2O_3/air-gap structures on (001) β-Ga_2O_3 substrate.

Second, a 119-nm-thick SiO_2 layer was deposited on the surface using PECVD. Third, the SiO_2 layer was patterned via laser lithography and CCP-RIE to open etching windows for the subsequent HCl gas etching. Fourth, the mesas were undercut through lateral etching with HCl gas for 5 min. Finally, the SiO_2 mask was removed by BHF etching.

After HCl gas etching, the resulting cantilevers and air bridges were examined by SEM, as shown in Figure 4. Figure 4(a1) and 4(a2) show SEM images of the cantilever and air-bridge structures with the SiO_2 mask still in place, respectively. Shadow regions observed beneath these structures suggest the formation of air gaps. In contrast, no such shadowed regions were observed along the etched sidewalls of the anchor regions due to a very low lateral etch rate of 0.07 μm min^{-1} along the [$\bar{1}$00] direction [Figure 2(d)], which is attributed to the high etch resistance of the (100) plane. The presence of air gaps was confirmed by cross-sectional observations at the centers of the cantilever and air bridge, as shown in Figure 4(b1) and 4(b2). Air gaps of approximately 0.5 μm and 0.6 μm were clearly observed beneath the cantilever and air bridge, respectively. The slightly narrower air gap under the cantilever is likely attributed to its downward bending compared to the air bridge. The thicknesses of the cantilever and air bridge were reduced to ~0.6 μm from their original mesa heights of 0.92 μm, due to etching from the reverse side of the mesas. Figure 4(c1) and 4(c2) show the cantilever and air bridge after the removal of the SiO_2 mask, respectively, demonstrating our state-of-the-art fabrication technique for β-Ga_2O_3/air-gap structures. Aside from the air-gap structures, the morphology of the etched bottom surface was slightly rough due to HCl gas etching. This implies that the reverse sides of the cantilevers and air bridges may also exhibit similar surface roughness. Therefore, further optimization is required to achieve improved surface smoothness, and this will be addressed in future work.

4. Summary

This study revealed significant anisotropy in the HCl gas etching of (001) β-Ga_2O_3 with lateral etch rates reaching up to 0.70 μm min^{-1} along the < 010 > direction-seven times greater than the vertical etch rate of 0.10 μm min^{-1}. Taking advantage of this high lateral-to-vertical etch rate ratio, we demonstrated the direct fabrication of cantilevers and air bridges, fundamental mechanically suspended structures for MEMS applications. Considering that most vertical power devices are fabricated on (001)-orientated substrates, the HCl

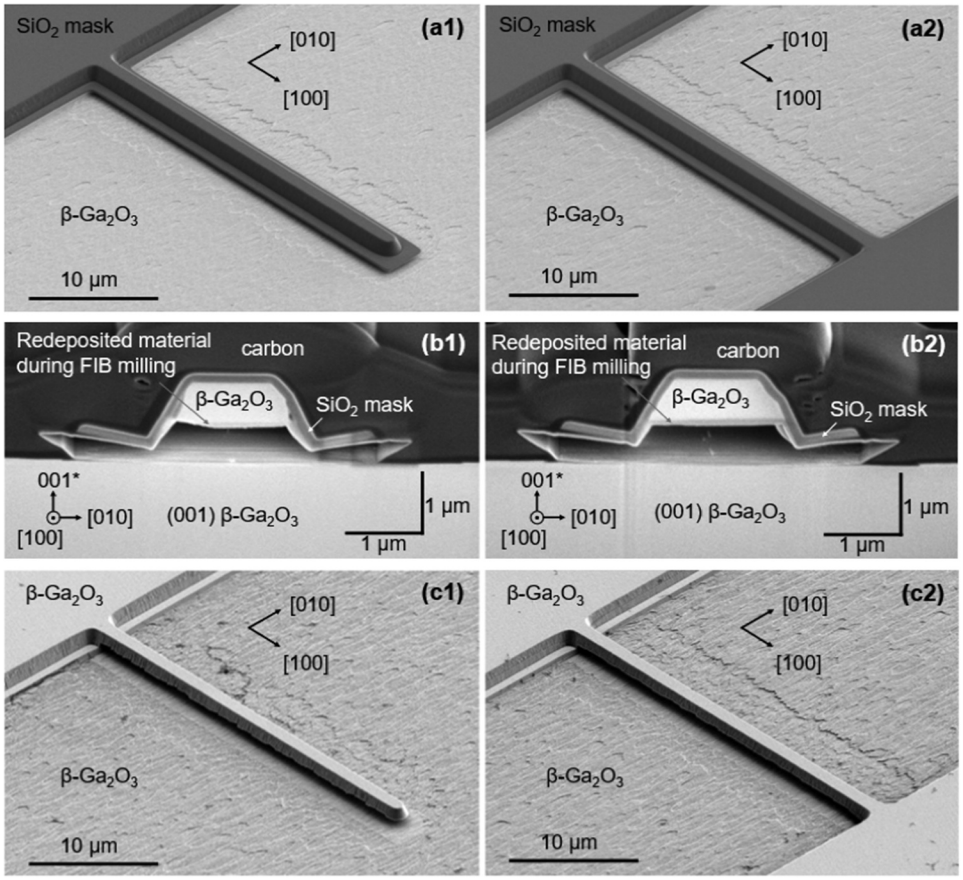

Figure 4. Summary of 54° tilted-view SEM images of the fabricated (a1)–(c1) cantilever and (a2)–(c2) air bridge structures on (001) β-Ga_2O_3 substrates. Images (a1) and (a2) were acquired after etching with HCl gas. Images (b1) and (b2) show cross-sectional views corresponding to (a1) and (a2), respectively. Images (c1) and (c2) were taken after the removal of the SiO_2 mask.

gas etching method presented here is particularly promising for the monolithic integration of MEMS and power devices.

Lastly, it is worth noting that a variety of crystallographic anisotropic etching techniques have been reported for β-Ga_2O_3, including hot phosphoric acid etching [27–29], photoelectrochemical etching [30,31], metal-assisted chemical etching [32,33], hydrogen-environment anisotropic thermal etching [34], forming gas etching [18], Ga flux etching [35], triethylgallium gas etching [36], and tert-butyl chloride gas etching [37]. Although our study focused on HCl gas etching, the air-gap formation demonstrated here might also be achievable using these alternative methods. However, further investigation should be required – particularly to determine the conditions under which the lateral etching rate becomes sufficiently high relative to the vertical etching rate.

Acknowledgements

All experiments, except for HCl gas etching, were conducted using equipment in the Nanofabrication and Electron Microscopy Units at the National Institute for Materials Science (NIMS), under the framework of the Advanced Research Infrastructure for Materials and Nanotechnology (ARIM), supported by the Ministry of Education, Culture, Sports, Science and Technology (MEXT), Japan (No. JPMXP1225NM5079).

Disclosure statement

No potential conflict of interest was reported by the author(s).

Funding

This work was financially supported by a Grant-in-Aid for Scientific Research (B) from the Japan Society for the Promotion of Science (JSPS), MEXT, Japan [JP24K01368].

ORCID

Takayoshi Oshima http://orcid.org/0000-0001-8550-9735
Yuichi Oshima http://orcid.org/0000-0001-8293-4891

References

[1] Higashiwaki M, Sasaki K, Kuramata A, et al. Gallium oxide (Ga_2O_3) metal-semiconductor field-effect transistors on single-crystal β-Ga_2O_3 (010) substrates.

Appl Phys Lett. 2012;100(1):013504. doi: 10.1063/1.3674287
[2] Kuramata A, Koshi K, Watanabe S, et al. High-quality β-Ga_2O_3 single crystals grown by edge-defined film-fed growth. Jpn J Appl Phys. 2016;55(12):1202A2. doi: 10.7567/JJAP.55.1202A2
[3] Sasaki K. Prospects for β-Ga_2O_3: now and into the future. Appl Phys Express. 2024;17(9):090101. doi: 10.35848/1882-0786/ad6b73
[4] Chen H, Li Z, Zhang Z, et al. Review of β-Ga_2O_3 solar-blind ultraviolet photodetector: growth, device, and application. Semicond Sci Technol. 2024;39(6):063001. doi: 10.1088/1361-6641/ad42cb
[5] Zhai H, Wu Z, Fang Z. Recent progress of Ga_2O_3 -based gas sensors. Ceram Int. 2022;48(17):24213. doi: 10.1016/j.ceramint.2022.06.066
[6] Zheng X-Q, Zhao H, Feng PXL. A perspective on β-Ga_2O_3 micro/nanoelectromechanical systems. Appl Phys Lett. 2022;120(4):040502. doi: 10.1063/5.0073005
[7] Zheng X-Q, Lee J, Rafique S, et al. Ultrawide band gap β-Ga_2O_3 nanomechanical resonators with spatially visualized multimode motion. ACS Appl Mater Interface. 2017;9(49):43090. doi: 10.1021/acsami.7b13930
[8] Zheng X-Q, Lee J, Rafique S, et al. β-Ga_2O_3 NEMS oscillator for real-time middle ultraviolet (MUV) light detection. IEEE Electron Device Lett. 2018;39(8):1230. doi: 10.1109/LED.2018.2850776
[9] Zheng X-Q, Xie Y, Lee J, et al. Beta gallium oxide (β-Ga_2O_3) nanoelectromechanical transducer for dual-modality solar-blind ultraviolet light detection. APL Mater. 2019;7(2):022523. doi: 10.1063/1.5054625
[10] Zheng X-Q, Kaisar T, Feng PX-L. Electromechanical coupling and motion transduction in β-Ga_2O_3 vibrating channel transistors. Appl Phys Lett. 2020;117(24):243504. doi: 10.1063/5.0031503
[11] Zheng X-Q, Zhao H, Jia Z, et al. Young's modulus and corresponding orientation in β-Ga_2O_3 thin films resolved by nanomechanical resonators. Appl Phys Lett. 2021;119(1):013505. doi: 10.1063/5.0050421
[12] Sui W, Enamul Hoque Yousuf SM, Liu Y, et al. Surface adsorption and air damping behavior of β-Ga_2O_3 nanomechanical resonators. Adv Mater Technol. 2024;9(5):2301356. doi: 10.1002/admt.202301356
[13] Xu W, You T, Mu F, et al. Thermodynamics of ion-cutting of β-Ga_2O_3 and wafer-scale heterogeneous integration of a β-Ga_2O_3 thin film onto a highly thermal conductive SiC substrate. ACS Appl Electron Mater. 2022;4(1):494. doi: 10.1021/acsaelm.1c01102
[14] Oshima T, Oshima Y. Plasma-free dry etching of (001) β-Ga_2O_3 substrates by HCl gas. Appl Phys Lett. 2023;122(16):162102. doi: 10.1063/5.0138736
[15] Oshima Y, Oshima T. Effect of the temperature and HCl partial pressure on selective-area gas etching of (001) β-Ga_2O_3. Jpn J Appl Phys. 2023;62(8):080901. doi: 10.35848/1347-4065/acee3b
[16] Oshima T, Oshima Y. Anisotropic non-plasma HCl gas etching of a (010) β-Ga_2O_3 substrate. Appl Phys Express. 2023;16(6):066501. doi: 10.35848/1882-0786/acdbb7
[17] Oshima T, Oshima Y. Using selective-area growth and selective-area etching on (−102) β-Ga_2O_3 substrates to fabricate plasma-damage-free vertical fins and trenches. Appl Phys Lett. 2024;124(4):042110. doi: 10.1063/5.0186319
[18] Oshima T, Togashi R, Oshima Y. Plasma-free anisotropic selective-area etching of β-Ga_2O_3 using forming gas under atmospheric pressure. Sci Technol Adv Mater. 2024;25(1):2378683. doi: 10.1080/14686996.2024.2378683
[19] Oshima T, Oshima Y. Near-vertical plasma-free HCl gas etching on (011) β-Ga_2O_3. Jpn J Appl Phys. 2025;64(1):018003. doi: 10.35848/1347-4065/ada706
[20] Oshima T, Oshima Y. Fabrication of air bridges on (100) β-Ga_2O_3 using crystallographic HCl gas etching. AIP Adv. 2025;15(5):055207. doi: 10.1063/5.0260753
[21] Mu S, Wang M, Peelaers H, et al. First-principles surface energies for monoclinic Ga_2O_3 and Al_2O_3 and consequences for cracking of $(Al_xGa_{1-x})_2O_3$. APL Mater. 2020;8(9):091105. doi: 10.1063/5.0019915
[22] Schewski R, Baldini M, Irmscher K, et al. Evolution of planar defects during homoepitaxial growth of β-Ga_2O_3 layers on (100) substrates—a quantitative model. J Appl Phys. 2016;120(22):225308. doi: 10.1063/1.4971957
[23] Schewski R, Lion K, Fiedler A, et al. Step-flow growth in homoepitaxy of β-Ga_2O_3 (100)—the influence of the miscut direction and faceting. APL Mater. 2019;7(2):022515. doi: 10.1063/1.5054943
[24] Jiang T, Wang H, Zhu H, et al. Single-crystalline β-Ga_2O_3 homoepitaxy on a near van der Waals surface of (100) substrate. Adv Sci. 2025;12(17):2417436. doi: 10.1002/advs.202417436
[25] Murakami H, Nomura K, Goto K, et al. Homoepitaxial growth of β-Ga_2O_3 layers by halide vapor phase epitaxy. Appl Phys Express. 2015;8(1):015503. doi: 10.7567/APEX.8.015503
[26] Geller S. Crystal structure of β-Ga_2O_3. J Chem Phys. 1960;33(3):676. doi: 10.1063/1.1731237
[27] Oshima T, Okuno T, Arai N, et al. Wet etching of β-Ga_2O_3 substrates. Jpn J Appl Phys. 2009;48(4R):040208. doi: 10.1143/JJAP.48.040208
[28] Zhang Y, Mauze A, Speck JS. Anisotropic etching of β-Ga2O3 using hot phosphoric acid. Appl Phys Lett. 2019;115(1):013501. doi: 10.1063/1.5093188
[29] Rebollo S, Itoh T, Krishnamoorthy S, et al. Heated-H3PO4 etching of (001) β-Ga_2O_3. Appl Phys Lett. 2024;125(1):012102. doi: 10.1063/5.0209222
[30] Jang S, Jung S, Beers K, et al. A comparative study of wet etching and contacts on (-201) and (010) oriented β-Ga_2O_3. J Alloys Compd. 2018;731:118–125. doi: 10.1016/j.jallcom.2017.09.336
[31] Choi YH, Baik KH, Kim S, et al. Photoelectrochemical etching of ultra-wide bandgap β-Ga_2O_3 semiconductor in phosphoric acid and its optoelectronic device application. Appl Surf Sci. 2021;539(15):148130. doi: 10.1016/j.apsusc.2020.148130
[32] Kim M, Huang H-C, Kim JD, et al. Nanoscale groove textured β-Ga_2O_3 by room temperature inverse metal-assisted chemical etching and photodiodes with enhanced responsivity. Appl Phys Lett. 2018;113(22):222104. doi: 10.1063/1.5053219
[33] Huang H, Kim M, Zhan X, et al. High aspect ratio β-Ga_2O_3 fin arrays with low-interface charge density by inverse metal-assisted chemical etching. ACS Nano. 2019;13(8):8784. doi: 10.1021/acsnano.9b01709
[34] Sato S, Momma T, Aikawa T, et al. Fabrication of mesa-shaped high-aspect Ga_2O_3/air DBR structures for optical integrated platform by HEATE method. In: The 5th International Workshop on Gallium Oxide and Related Materials, Porc; Berlin (Germany); 2024. p. WeP_35.

[35] Kalarickal NK, Fiedler A, Dhara S, et al. Planar and three-dimensional damage-free etching of β-Ga_2O_3 using atomic gallium flux. Appl Phys Lett. 2021;119 (12):123503. doi: 10.1063/5.0057203
[36] Katta A, Alema F, Brand W, et al. Demonstration of MOCVD based in situ etching of β-Ga_2O_3 using TEGa. J Appl Phys. 2024;135(7):075705. doi: 10.1063/5.0195361
[37] Gorsak CA, Bowman HJ, Gann KR, et al. In situ etching of β-Ga_2O_3 using tert-butyl chloride in an MOCVD system. Appl Phys Lett. 2024;125(24): 242103. doi: 10.1063/5.0239152